07

Application of uncooled microbolometers for detecting pulsed terahertz and infrared radiation

© M.A. Dem'yanenko,[1] V.V. Startsev[2]

[1] Rzhanov Institute of Semiconductor Physics, Siberian Branch, Russian Academy of Sciences,
630090 Novosibirsk, Russia
[2] Joint Stock Company „Optical Mechanical Design Bureau Astron",
140080 Lytkarino, Moscow Oblast, Russia
e-mail: demyanenko@isp.nsc.ru

Received June 21, 2021
Revised November 17, 2021
Accepted November 26, 2021

Analytical relations for temperature response of the bolometer to periodic radiation pulses are obtained. It is theoretically shown and experimentally confirmed by the example of infrared bolometers that when detecting short radiation pulses, in contrast to the case of constant radiation, increasing the thermal conductivity of the bolometer and, accordingly, decreasing its thermal relaxation time, it is possible to significantly increase the response rate of the receiver, practically without reducing its sensitivity. The possibility of effective registration of pulsed terahertz radiation by microbolometers with a resistively coupled, thermally non-isolated antenna is considered. It is shown that such bolometers, which have increased thermal conductivity and, accordingly, reduced sensitivity to continuous-wave radiation, can be highly effective when detecting pulsed radiation with a duration shorter than the thermal relaxation time of the bolometer. On their basis, uncooled matrix detectors of pulsed terahertz radiation, characterized by a minimum detectable energy of less than $1 \cdot 10^{-12}$ J and a frame rate of up to 1000 Hz, can be developed.

Keywords: microbolometer, pulsed terahertz radiation, antenna.

DOI: 10.21883/TP.2022.03.53266.190-21

Introduction

Matrix uncooled microbolometer detectors are traditionally applied in the systems of registration of infrared (IR) [1,2] and terahertz (THz) radiation [3–9] with constant or slowly varying intensity, i.e. when characteristic time of variation of radiation power that falls on the detector is considerably higher than the time of thermal relaxation of bolometers. However, in a series of cases application of pulsed radiation enables improvement of the accuracy of measurement as a result of elimination of constant or low-frequency parasitic signals. In some tasks, e.g., in case of the need for registration of THz radiation reflected from remote objects, a powerful radiation highlighting is required. In such cases, low duration pulsed radiation is applied in order to decrease energy consumption and to improve safety, the same as it is applied for remote atmosphere sensing [10,11]. In addition, some sources of THz radiation, e.g., based on photoconductive antennas [12,13] and on non-linear optical crystals [14] have a pulsed mode of operation, or, similar to quantum cascade lasers [15–17], they have a considerably higher power in the pulsed mode of operation. On the one hand, application of uncooled microbolometer detectors for registration of pulsed signals requires an additional analysis of their operation specifics, and on the other hand, results in the need for review of the design approaches applicable in the development of the detectors themselves, in order to obtain high sensitivity to pulsed radiation. First of all, this regards THz range receivers, a high sensitivity in which is ensured, first, by application of antennas linked to a load located on thermally insulated membrane of the bolometer via the resistance or capacitance methods [8–9,18], and, second, by radiation absorbers based on thin metallic films [5,7] and the metamaterials [19] and applied to the bolometer membrane. The detectors with antennas can be subdivided into two types. The first type includes bolometers that combine application of the antenna placed on a pad and conjugated to a load via capacitance link, and the resistance-linked antenna placed onto a thermally insulated membrane of the bolometer [8–9]. Such detectors have a low thermal conductivity. The second type includes bolometers with the resistance-linked and thermally uninsulated (located on a pad) antenna [18]. Such detectors have a high thermal conductivity that is caused by a resistance link busbar between the antenna and a load. This makes them less sensitive to constant THz radiation, meanwhile, enabling them to act faster because of a less time for thermal relaxation. When registering pulsed radiation an impact of thermal conductivity to the value of signal is considerably mitigated, and such detectors could result high efficient.

This study deals with the dependences of the value of signal of the bolometer on the IR pulse or THz radiation parameters and the time of the bolometer thermal relaxation, based on theoretical and experimental approaches. The study covers main design specifics of manufacture of

uncooled matrix detectors based on the microbolometers with resistance-linked and thermally uninsulated antenna intended for efficient registration of pulsed terahertz radiation.

1. Temperature response of the bolometer under pulsed illumination

The heat balance equation of the bolometer under impact of absorbed radiation of signal to it, depending on the time t, and constant background, whose powers are $P_S(t)$ and P_B, accordingly, is as follows

$$C\frac{dT_D}{dt} = P_S(t) + P_B + Q_D(T_D) - G_0(T_D - T_C). \qquad (1)$$

Here, T_D and T_C are the temperature of the bolometer and a pad, on which it was manufactured; C and G_0 are thermal capacity and thermal conductivity of the bolometer, which, due to a low difference of T_D and T_C will be considered as depending on the temperature T_C only; Q_D is the Joule heat power released in the bolometer at the time of current is passing through it. It is assumed that the heat capacity and thermal conductivity of small heat insulating bars are far less than that of the bolometer membrane, thus ensuring evenness of its temperature, which we will take as the bolometer temperature T_D. Under impact of the signal radiation the bolometer resistance R_D and Q_D change, accordingly, thus leading to additional change of the temperature T_D as a result of so called thermoelectrical interaction or thermoelectrical feedback [20]. In case of switching the bolometer on serially with the DC voltage source V_0 and the loading resistance, whose value R_L does not depend on the power released in it, the change of power of the released Joule heat Q_D is expressed as the ratio $dQ_D(T_D) = \beta\alpha Q_{DO} dT_D$ [20,21]. Here, $\alpha = (dR_D/dT_D)/R_D$ is the temperature coefficient of resistance (TCR), $\beta = (R_L - R_{DO})/(R_L + R_{DO})$, R_{DO} and Q_{DO} are the values R_D and Q_D at the operating temperature of the bolometer T_O determined by the ratio of $T_O = T_C + (P_B + Q_{DO})/G_0$. With the breakdown of $Q_D(T_D)$ into the Taylor's series close to operating point T_O to first-order terms, the ratio (1) can be written as [20]:

$$\frac{dT}{dt} + \frac{T}{\tau} = \frac{P_S(t)}{C}. \qquad (2)$$

Here, $T = T_D - T_O$ is the bolometer response to the signal radiation, $\tau = C/G$ and G are efficient time of the bolometer thermal relaxation and efficient thermal conductivity specified by the ratio $G = G_0 - \beta\alpha Q_{DO} = G_0(1 - \beta\alpha T_{QO})$, $T_{QO} = Q_{DO}/G_0$ is the value of bolometer heating up due to the Joule heat released in the operating point. The value αT_{QO} can be of the order of unity. In fact, bolometer heating up, whose resistance R_D, TCR α and thermal conductivity G_0 are 100 kΩ, 2%/K and 10^{-7} W/K [2,21], will be approximately 25 K ($\alpha T_{QO} = -0.5$) at the bolometer voltage bias $V_D = V_0 R_{DO}/(R_L + R_{DO}) = 0.5$ V. Note that the equation (2) allows, on the one hand, to find the time dependence of the temperature response of the bolometer $T(t)$ based on the specified dependence of the power of absorbed signal radiation on the time $P_S(t)$, and, on the other hand — to determine the dependence of the signal power on the time $P_S(t)$ based on the measured dependence $T(t)$. In particular, at the constant power of signal P_S it will result $T = P_S\tau/C = P_S/G$.

General solution of the equation (2) is [22]:

$$T(t) = T(t_0)\exp\left(-\frac{t - t_0}{\tau}\right) + \int_{t_0}^{t} \frac{P_S(t')}{C}\exp\left(-\frac{t - t'}{\tau}\right)dt', \qquad (3)$$

where $T(t_0)$ is the value T at some instant t_0. If radiation has periodic time dependence with the period Θ, then for any t_0 the parity $T(t_0 + \Theta) = T(t_0)$ is true. Together with the ratio (3) it enables to get that

$$T(t_0) = \frac{\exp(-\Theta/\tau)}{[1 - \exp(-\Theta/\tau)]} \int_{t_0}^{t_0+\Theta} \frac{P_S(t')}{C}\exp\left(\frac{t' - t_0}{\tau}\right)dt'. \qquad (4)$$

In case of a pulsed radiation, where $P_S(t)$ is not zero only within the interval $t_1 < t < t_2$ ($t_1 = t_S - t_{pe}/2$, $t_2 = t_S + t_{pe}/2$, t_S is the moment of time of a conventional midpoint of the pulse arrival, t_{pe} is efficient pulse duration), the ratios (4) and (3) are transformed into

$$T(t_1) = DT(t_1, t_2)\frac{\exp(-\Theta/\tau)}{[1 - \exp(-\Theta/\tau)]}\exp\left(-\frac{t_1 - t_S}{\tau}\right), \quad (5)$$

$$T(t) = T(t_1)\exp\left(-\frac{t - t_1}{\tau}\right) + DT(t_1, t)\exp\left(-\frac{t - t_S}{\tau}\right), \quad \text{at} \quad t_1 < t < t_2, \qquad (6a)$$

$$T(t) = DT(t_1, t_2)\frac{1}{[1 - \exp(-\Theta/\tau)]}\exp\left(-\frac{t - t_S}{\tau}\right). \quad \text{at} \quad t_2 < t < t_1 + \Theta, \qquad (6b)$$

where

$$DT(t_1, t) = \int_{t_1}^{t} \frac{P_S(t')}{C}\exp\left(\frac{t' - t_S}{\tau}\right)dt'. \qquad (7)$$

If $t_{pe} \ll \tau$, then, by making the breakdown of the ratio (7) in series by a low parameter t_{pe}/τ and ignoring the first-order and senior-order terms, we will find that $DT(t_1, t) \approx Q_S(t)/C$ and $DT(t_1, t_2) \approx Q_S/C$, where Q_S and $Q_S(t)$ are the energies of the radiation pulse absorbed within the whole pulse duration and within the time interval $t_1 - t$, accordingly. For the radiation pulse symmetrical relative to the point t_S the above mentioned breakdown $DT(t_1, t_2)$ will not include the first-order terms, therefore, the ratios (5) and (6b) describing the temperature response $T(t)$ at the moments of time between the pulses, after $DT(t_1, t_2)$ is replaced with Q_S/C in them, will have

the accuracy of the second-order infinitesimal of t_{pe}/τ. In this case, for the temperature response prior to pulse arrival and after it has passed, it is:

$$T(t_1) \approx (Q_S/C)\exp[-(t_1-t_S)/\tau)]/[\exp(\Theta/\tau)-1],$$

$$T(t_2) \approx (Q_S/C)\exp[-(t_2-t_S)/\tau)]/[1-\exp(-\Theta/\tau)],$$

and its increment during the pulse will be

$$T(t_2)-T(t_1) \approx (Q_S/C)\,\mathrm{sh}[(\Theta-t_{pe})/2\tau]/\,\mathrm{sh}(\Theta/2\tau)$$

$$\approx (Q_S/C)[1-(t_{pe}/2\tau)\,\mathrm{cth}(\Theta/2\tau)].$$

It can be seen from the last ratio, that, if Θ is higher or about τ and $t_{pe} \ll \tau$, then $T(t_2)-T(t_1) \approx Q_S/C$. It means that all radiation pulse energy absorbed by the bolometer is spent to heating it, and the heat loss during the pulse due to the bolometer thermal conductivity can be ignored. If $\Theta \ll \tau$, then

$$T(t_1) \approx (Q_S/C)(\tau/\Theta)(1+t_{pe}/2\tau)/(1+\Theta/2\tau),$$

$$T(t_2) \approx (Q_S/C)(\tau/\Theta)(1-t_{pe}/2\tau)/(1-\Theta/2\tau)$$

and

$$T(t_2)-T(t_1) \approx (Q_S/C)(1-t_{pe}/\Theta).$$

In this case, the bolometer temperature increment of Q_S/C during the pulse will require compliance with a more strict condition $t_{pe} \ll \Theta \ll \tau$. It is because that at $\Theta \ll \tau$ prior to arrival of another radiation pulse, the bolometer fails to cooldown after several impacts to it from previous pulses irradiating the bolometer during its thermal relaxation time τ, the number of which can be estimated as the value τ/Θ. As a result the bolometer is heated up to the temperature $T(t_1) \sim (Q_S/C)(\tau/\Theta) \gg Q_S/C$. In this situation the heat loss rate due to thermal conductivity G is increased τ/Θ times versus the case $\Theta > \tau$, when the bolometer has considerably cooled down prior to arrival of the next pulse, therefore resulting in the need for decrease of the pulse duration also τ/Θ times, in order to make the energy loss within the pulse duration far less than the absorbed radiation pulse energy. Note that $(Q_S/C)(\tau/\Theta) = \langle P_S\rangle/G$, where $\langle P_S\rangle = Q_S/\Theta$ is the radiation power averaged for the period and, therefore, in zero approximation by t_{pe}/τ and Θ/τ we determine that $T(t_1) \approx T(t_2) \approx \langle P_S\rangle/G$.

In general case, when the efficient radiation pulse duration t_{pe} can be comparable to the time of thermal relaxation τ, the heat loss during the radiation pulse duration due to thermal conductivity G could become considerable even at $\Theta \gg \tau$ and for calculation of the values $DT(t_1,t)$ and $DT(t_1,t_2)$ the integral expression (7) must be used.

For illustration of the information given above, consider the dependences of the bolometer temperature response on time under impact on it of three types of the pulsed radiation (Fig. 1) having similar full energy Q_S and symmetrical

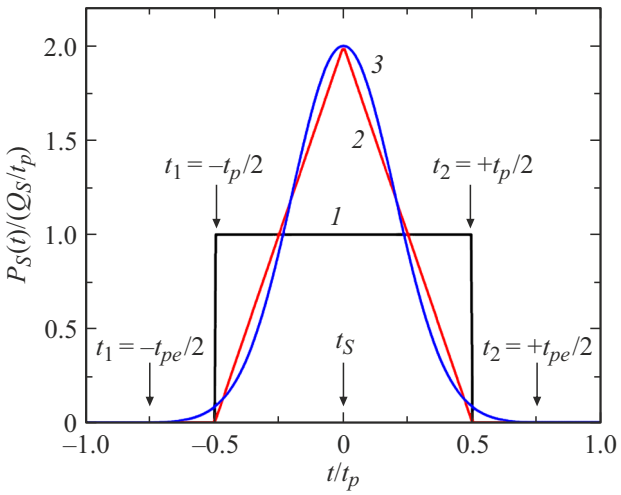

Figure 1. Rated dependences of the radiation power absorbed by the bolometer $P_S(t)$ on the time t for the radiation pulses of various shape: *1* — rectangular, *2* — triangular, *3* — Gauss, used in calculation of the temperature response of the bolometer shown in Fig. 2; t_S is the moment of arrival of the pulse midpoint, t_p is the parameter specifying the pulse duration, t_1 and t_2 specify the time interval, beyond which the $P_S(t)$ is considered as zero, $t_{pe} = t_2-t_1$ is efficient pulse duration.

relative to the moment of their midpoint arrival t_S taken as zero:

1) rectangular pulse:

$$P_S(t) = Q_S/t_p \text{ at } -t_p/2 < t < t_p/2, \tag{8a}$$

2) triangular pulse:

$$P_S(t) = 2(Q_S/t_p)[1-|t/(t_p/2)|], \quad -t_p/2 < t < t_p/2, \tag{8b}$$

3) Gauss pulse:

$$P_S(t) = \frac{Q_S}{\sqrt{2\pi}(t_p/b)}\exp\left[\frac{-t^2}{2(t_p/b)^2}\right], \text{ where } b = 2\sqrt{2\pi}. \tag{8c}$$

For rectangular and triangular pulses the power of absorbed radiation $P_S(t)$ is not equal to zero only between $t_1 = -t_p/2$ and $t_2 = t_p/2$, i.e. in this case the efficient pulse duration t_{pe}, beyond which the power of falling radiation $P_S(t)$ is equal to zero, could be taken as t_p. In case of Gauss pulse the remainder of distribution of $P_S(t)$ extends also out of the interval $-t_p/2 < t < t_p/2$, this is why one should select $t_1 = -n(t_p/2)$, $t_2 = n(t_p/2)$ and $t_{pe} = nt_p$, where n is equal to, for example, 1.5. Then, we may consider, that beyond the interval (t_1,t_2) $P_S(t)$ is equal to zero at a higher accuracy $[P_S(t_1)/P_S(0) = P_S(t_2)/P_S(0) \approx 8.5\cdot 10^{-4}]$. Note, that in case of three pulses given above, that are often used in practice, it is succeeded to get analytical expression for $DT(t_1,t)$ and $DT(t_1,t_2)$, which are given in Appendix and could be useful, for example, in case

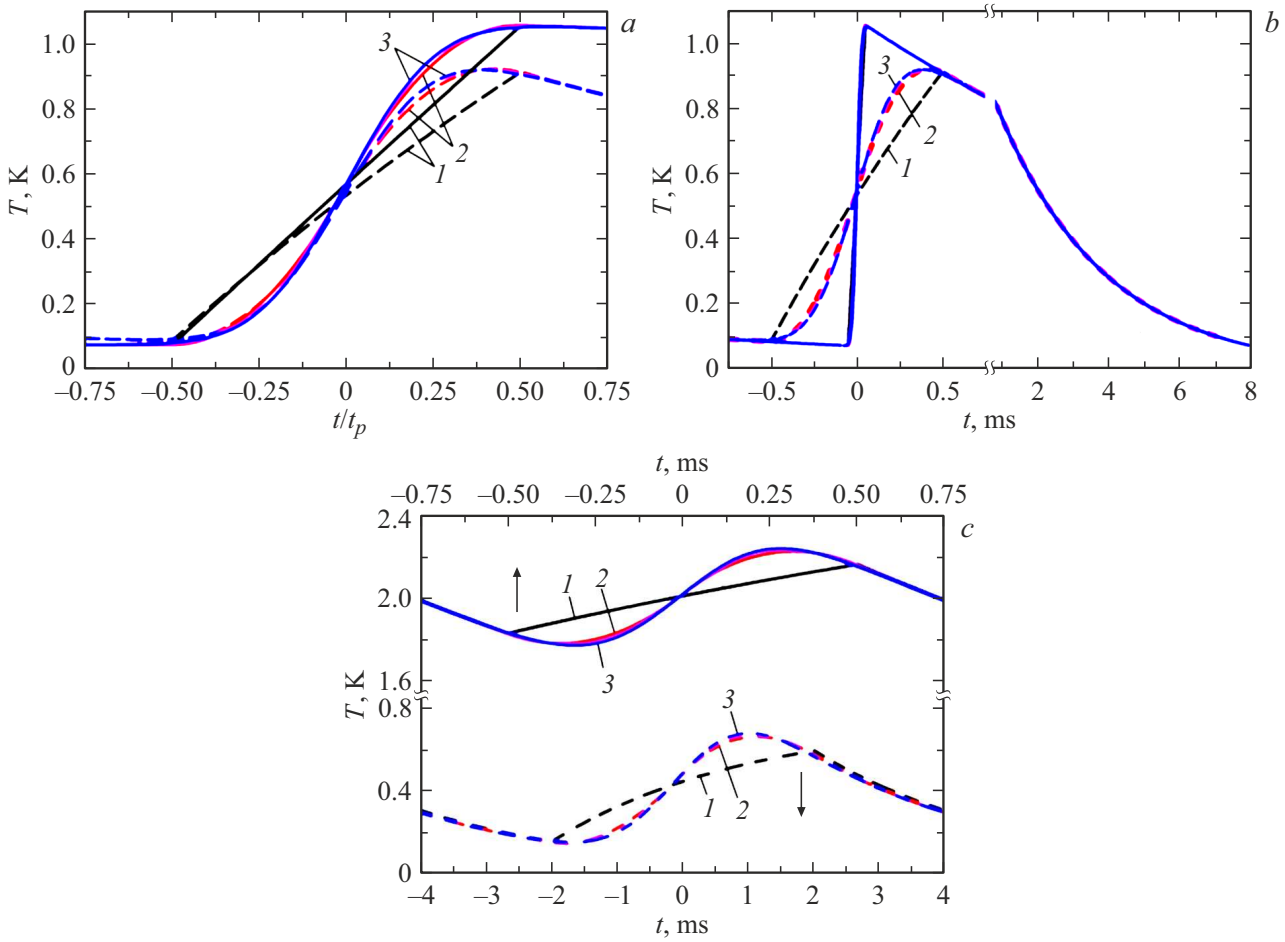

Figure 2. Dependences of the temperature response of the bolometer T on time t under impact of the pulsed radiation of various shape, pulse duration t_p and its period of passing Θ: $t_p = 0.1$ ms (solid), $t_p = 1$ ms (dashed), $\Theta = 8$ ms (a, b); $t_p = 1$ ms and $\Theta = 1.5$ ms (solid), $t_p = 4$ ms and $\Theta = 8$ ms (dashed) (c). The pulse shape in all figures is stated as digits: *1* — rectangular, *2* — triangular, *3* — Gauss. The absorbed energy of the radiation pulse $Q_S = 1$ nJ, the time of the bolometer thermal relaxation $\tau = 3$ ms, the bolometer thermal capacity $C = 1$ nJ/K.

of the need for fast calculations and analysis of impact of the radiation pulse parameters and of the bolometer itself to the value and shape of the temperature response.

The dependences of temperature response of the bolometer T on the time t under impact to it of the three types of pulsed radiation given above, calculated by the ratios (5)–(7), are given in Fig. 2. How can be seen on the graphs, if t_p is low enough versus τ and Θ, then the difference of temperatures immediately after the pulse $T(t_2)$ has passed and immediately prior to its arrival $T(t_1)$ is approximately equal to Q_S/C, and the accuracy of this equation is increased as far as t_p/τ decreases (Fig. 2, *a, b*). In this case the heat loss to the pad during the pulse is low. If the period Θ is considerably higher than t_p and τ, then the bolometer has fully cooled down before arrival of the next pulse (Fig. 2, *b*). At $\Theta < \tau$ the bolometer fails to cool down between the pulses, and, in accordance with the above, the temperature response $T(t_1)$ prior to arrival of the next pulse, which is determined generally by the mean radiation power Θ, could appear to be considerably higher than the value Q_S/C (solid curves in Fig. 2, *c*). This increases the heat loss into the pad, as a result of which the temperature response increment during the pulse $T(t_2)-T(t_1)$ appears to be far less than Q_S/C (if no condition $t_p \ll \Theta$ is met) even if $t_p \ll \tau$ (solid curves in Fig. 2, *c*). It is important to note, that in accordance with the above, the temperature responses T measured between the radiation pulses at similar values of time $t-t_S$ have a low dependence on the shape and duration of pulses, if their period is similar and $t_p \ll \tau$ (Fig. 2, *b*). It is fair even in cases, when the heat loss during the pulse is not low (solid curves in Fig. 2, *c*). Note also that for triangular and Gauss pulses, the maximum values of temperature are achieved before the end of the pulse. It is especially clear in cases, when the heat loss into the pad during the pulse is considerable (Fig. 2, *c*).

2. Experimental study of dependence of the bolometer signal on the time of thermal relaxation at pulsed illumination

The study deals with the response of a matrix microbolometer detector (MMBD) to the pulsed IR radiation depending on the value of the thermal relaxation time of the bolometer τ, which varied by changing the pressure inside the vacuum housing of the detector. The signals from the MMBD elements were read line by line at the frame rate 25 Hz, so that the measurement of the elements of each next line was performed $40\,\text{ms}/241 = 166\,\mu\text{s}$ after measurement of the previous one. (In the process of the signals reading from the MMBD with the format 320×240 one „service" line was added.) Therefore, having illuminated a column of microbolometers uniformly with the pulsed radiation and having recorded the current frame signals read from the MMBD into a file, we can measure the time dependence of the microbolometers response to the pulsed radiation.

In the line-by-line signals reading from the MMBD the bolometers offset was performed within $30\,\mu\text{s}$ one time per frame (i.e. once per 40 ms). For the rest time no current is passing through the bolometer, therefore, dependence of the bolometer temperature on the time will be determined by the ratio (2), where $\tau = C/G_0$. Impact of thermoelectrical feedback occurs only during the bolometer offset pulse application. It results in the measured signal V_S relation with the signal V_{S0} calculated without considering thermoelectrical feedback, through the following ratio: $V_S = V_{S0}/(1-\beta\alpha T_{i0})$ [23]. Here, ΔT_{i0} is the bolometer heating up caused by the offset pulse, which at the bolometer voltage bias $V_D = 2\,\text{V}$ (other parameters remain the same: $R_D = 100\,\text{k}\Omega$, $\alpha = -2\%/\text{K}$ and $C = 1\,\text{nJ/K}$) appears to be equal to 1.2 K, so the correction $\beta\alpha T_{i0}$ can be ignored. In the matrix microbolometer detector used in the experiment the bridge measurement was applied, where $R_D \approx R_L$, therefore, $\beta \approx 0$, which additionally decreases impact of the thermoelectrical feedback.

The IR radiation pulse was generated as follows (Fig. 3). The reference long emitter of the type „absolute black body" (ABB) of the brand AChT-4I, with the diameter 75 mm *1* heated up to the temperature of 90°C, was placed behind the slit diaphragm *2* with the width of 8 mm, in front of which there is rotating disc *3* of modulator with slot *4* having the width of 6 degrees of arc, located at the distance from the rotation axis 60 to 90 mm. The slot diaphragm image was focused on the MMBD with the format 320×240 and the pixel size $51\,\mu\text{m}$, manufactured in the Rzhanov Institute of Semiconductor Physics, Siberian Branch of the Russian Academy of Sciences (Novosibirsk) [24]. Two illuminated areas were generated on the photosensitive field of the MMBD *5*, while the disc was rotating. One area *6* was illuminated by the radiation pulses passing through the slot *4*, and the second one *7* that corresponds to a part of the slit diaphragm *2* behind the edge of the rotating disc *3* was illuminated by constant (not modulated) radiation. By rotating the disc *3* slowly and measuring the signal for the column 171 of microbolometers shown in Fig. 3 by the line *8* and corresponding to the midpoint of the image of the slit diaphragm *2*, we determined dependence of the power of IR radiation on the disc rotation angle, therefore, the radiation pulse shape, which further was used in calculations. It was found that the angular width of the obtained distribution at the level of 10% is 1.5 times higher than the geometric width of the slot *4*. So, by rotating the disc at the frequency of 25 Hz the IR pulse duration at the line *8* was about $1.5 \cdot (40\,\text{ms}/60) = 1\,\text{ms}$, which is considerably less than the time of thermal relaxation of the MMBD bolometers at a high vacuum τ_0, which is 15 ms.

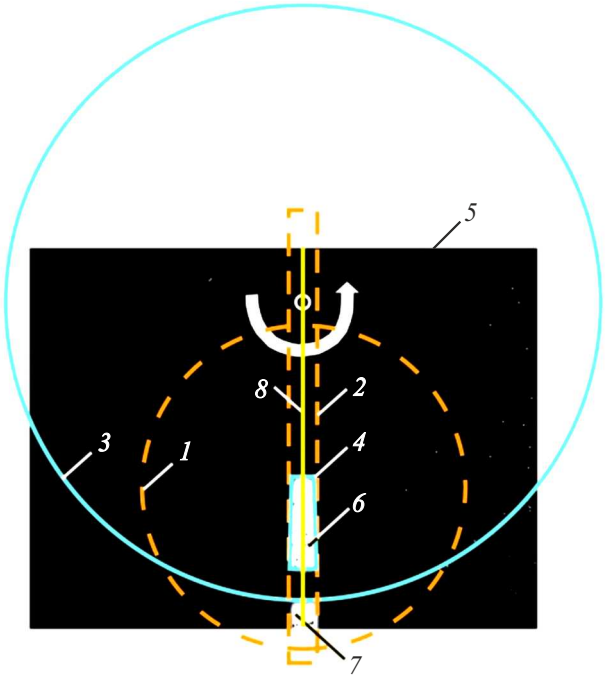

Figure 3. Schematic view of projections of absolute black body (*1*), slit diaphragm (*2*), modulator disc (*3*) and slot in it (*4*) on the sensitive field of the MMBD (*5*), where areas highlighted both by pulsed (*6*) and constant radiation (*7*) are formed. The signals were measured for the column of bolometers shown by the line (*8*). Dark field of the detector — no signal, white one — signal.

Figure 4 shows distributions of the signal values along the column 171 of MMBD (bottom scale) measured with the stationary *1* and rotating *2–5* disc at a high *1–3* and low *4, 5* vacuum. The time scale (top) is counted from the frame start (from „the service" line located before the first line). Distribution of signals measured at a high vacuum without disc rotation (position of the disc slot coincides the diaphragm slit) is quite uniform within the disc slot area (lines 145–205), which corresponds to uniform illumination along the measured column of microbolometers. The values of signal of microbolometers in the lines 220 to 240

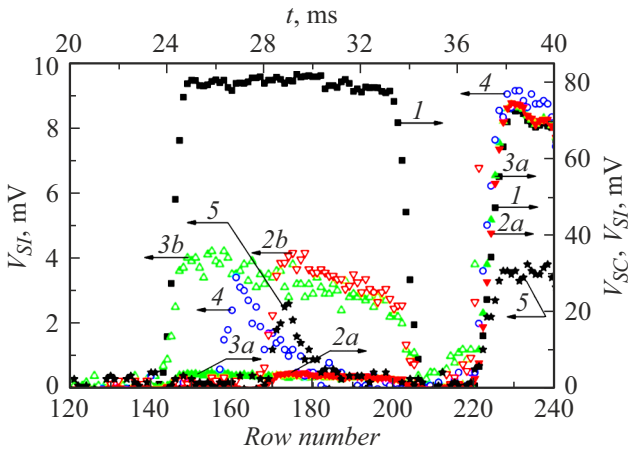

Figure 4. Distribution of the signal value by the column 171 of the MMBD with stationary (*1*) and rotating (*2–5*) disc at a high (*1–3*) and low (*4, 5*) vacuum. The top scale means the time dependence of signals in the pulse-highlighted area (lines 145–205).

corresponding to the area *7* shown in Fig. 3, which is always illuminated by constant (not modulated) radiation, is a bit less, possibly, due to uneven highlighting at the matrix edge. Note that because the frequency of MMBD frames reading and the disc rotation frequency were not synchronized against each other, the radiation pulse not always fell within the time interval of polling the lines within the pulse-illuminated area (lines 145–205), and, when it had fallen within — the pulse start position is quite arbitrary. Thus, for example, when measuring the dependence *2* the radiation pulse arrived at the moment of reading the line 170, and when measuring the dependence *3* — approximately, at the moment of reading the line 145 or a bit earlier.

When rotating the disc and with a high vacuum, the signal value within the disc slot area, illuminated by the pulses with the duration $t_p = 1$ ms, is considerably less than the signal within constantly illuminated area *7* shown in Fig. 3. It is because, in accordance with the information given in section 1, the bolometer signal V_{SI}, when illuminated by pulses with the duration $t_p \ll \tau$, is pro rata $P_S t_p/C$, meanwhile the signal V_{SC} under constant illumination is pro rata $P_S/G_0 = P_S\tau/C$. Therefore, as far as the thermal conductivity G_0 of the bolometer is increased (and as far as τ decreases, accordingly) the peak value V_{SI} does not depend on G_0, while $\tau > t_p$. It is very clear according to the experiment. The value of measured pulsed signal V_{SI} at a high vacuum exceeds the value of signal at a low vacuum insignificantly, meanwhile relevant signals V_{SC} within the constant illumination area differ 20 times, which corresponds to the increase G_0 (and decrease τ) 20 times. Such a high decrease τ is clear also from the dependence of the signal value V_{SI} on the time. At a high vacuum after the end of the radiation pulse the signal V_{SI} decreases about 1.5 times for 9 ms (curve *3* in Fig. 4), meanwhile at a low vacuum it is attenuated virtually in full for 2–3 ms (curve *5*).

Figure 5 shows experimental and theoretical dependences of the peak value of the MMBD signal on the value τ when it is irradiated by the IR radiation pulses. The time of thermal relaxation of bolometers was decreased as far as gas inflowed the vacuum housing of MMBD and the time was determined by the ratio $\tau = \tau 0(V_{SC}/V_{SC0})$; V_{SC0} and V_{SC} are the values of signal within the area of constant illumination (lines 220–240) at a high and low vacuum, accordingly. Theoretical dependences of the peak value of the signal V_{SI} on the value τ were calculated by the integral ratios (5)–(7), where the radiation pulse shape determined experimentally by measurement of the value of MMBD signals at slow disc rotation was used. Good match of experimental and calculated dependences for the radiation pulse with the duration 1 ms were obtained by taking the thermal capacity of the bolometer C equal to $1.2 \cdot 10^{-9}$ J/K (at that $G_0 = 0.8 \cdot 10^{-7}$ W/K), which corresponds to the characteristics values for the MMBD used in the experiment with the pixel size 51 μm [25]. In accordance with the above, the signal value has low variations while the time of thermal relaxation is considerably higher than the pulse duration. This feature allows developing detectors of short THz radiation pulses, based on application of the bolometers having low values of the time of thermal relaxation, which, in turn, allows increasing the frame rate and enables using the bolometers with resistance-linked and thermally uninsulated antenna, having a high thermal conductivity and, therefore, low sensitivity to constant radiation.

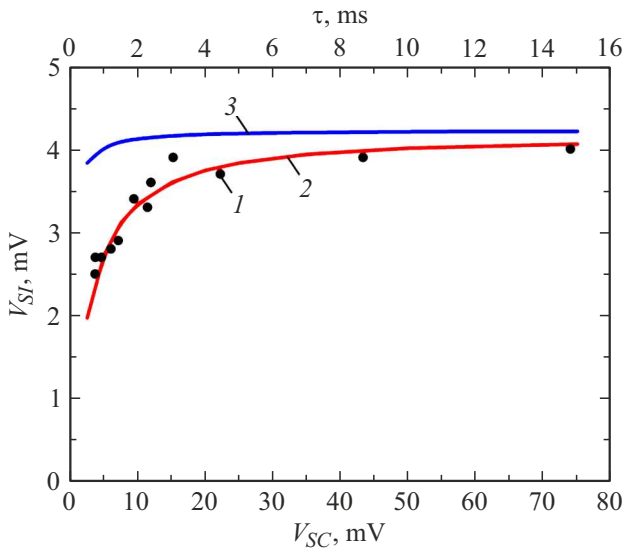

Figure 5. Experimental (*1*) and theoretical (*2, 3*) dependences of the peak value of MMBD signal V_{SI} on the thermal relaxation time τ (top scale) calculated through the values of signal V_{SC} within the constant illumination area (bottom scale) under irradiation by IR pulses with the duration 1 (*1, 2*) and 0.1 ms (*3*).

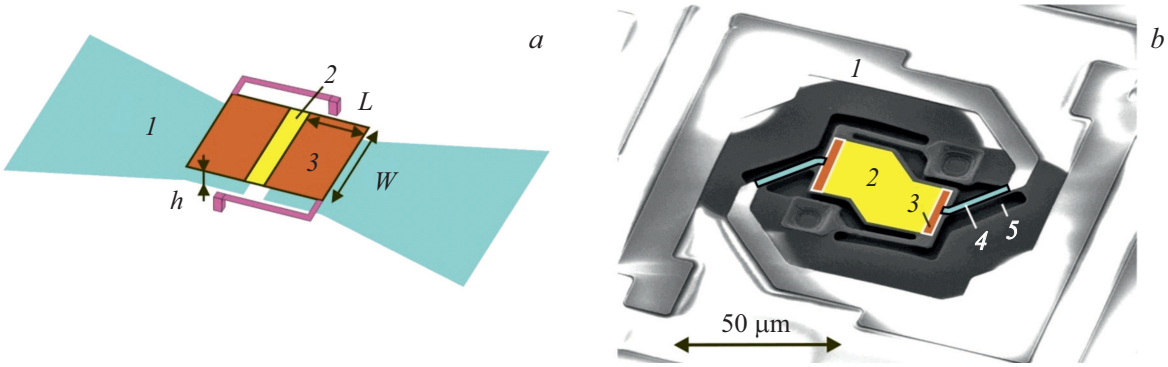

Figure 6. Antenna bolometers with the capacitance (*a*) and resistance link (*b*). *1* — antenna, *2* — load (heater), *3* — low-ohmic contact to the load and the capacitance link armature, *4* — busbar of the resistance link between the antenna and heater, *5* — area of etched sacrificial layer.

3. Uncooled microbolometer detectors of pulsed THz radiation with resistance-linked antennas

For the development of bolometers with antennas it is important to ensure efficient conjugation of the antenna and resistive load (heater), in which the energy of electromagnetic wave falling on the bolometer is released. Two conjugation methods are successfully applied within the THz range of frequencies. In the first method, the antenna is located directly on the thermally insulated membrane together with a load. In this case these are linked via direct, i.e. resistance method. In the second method, the antenna is placed onto a pad, above which a bolometer is suspended, and the link to a load located on the thermally insulated membrane of the bolometer is provided through the capacitance link via thin vacuum gap (Fig. 6, *a*). Generally, microbolometers that combine two variants are used [8,9]. Such structures are hard to apply for registration of radiation with the frequency less than 1 THz, since low radiation frequency impedes using the capacitance link, and high dimensions of the antenna do not allow placing it on a small (about $25 \times 25\,\mu$m) membrane of the bolometer or, otherwise, will result in a high thermal capacity of the bolometer. Truly, the impedance Z_C of the capacitance link between the antenna and load can be estimated as the value $2/(C_e\omega)$ corresponding to two capacities C_e connected in series with the load and formed by electrodes with the dimensions $W \times L \approx 25 \times 10\,\mu$m, separated by a vacuum gap $h \approx 2\,\mu$m (Fig. 6, *a*). At the frequencies $\omega/2\pi \approx 0.3$ THz the impedance $Z_C \approx 960\,\Omega$, which is considerably higher than the vacuum impedance equal to 377 Ω, and impedes harmonization of the antenna and a load, especially, for development of a broadband detector.

For the pulsed THz radiation detectors one can apply the resistance link between the antenna located on a pad (e.g., made of silicon, in which, in general, the signals reading scheme is provided — multiplexor), and a load located on the bolometer membrane (Fig. 6, *b*). In this case the load occupies virtually whole surface of the membrane, thus contributing into fast and even heating of thin membrane when absorbing the radiation pulse. The heat is distributed across the membrane and the characteristic time of heating up τ_d of the membrane made of silicon nitride with the thickness of $d = 0.3\,\mu$m is $\sim c\rho d^2/\kappa \approx 7 \cdot 10^{-8}$ s, where ρ, c and κ are the density, specific thermal capacity and thermal conductivity of silicon nitride equal to 2.2 g/cm^3, 1.5 J/gK and 0.045 W/cmK, accordingly [26]. Availability of low-ohmic contacts to the resistance load (Fig. 6, *b*), in which no heat is released, will result in uneven heat release, therefore, in redistribution of heat along the membrane. However, in case of a small width of such contacts ($a \approx 1\,\mu$m) and their positioning in perpendicular to the thermally sensitive layer, or with serial alternation of the contact stripes and resistive load (with the width of $a \approx 1\,\mu$m each), the impact of longitudinal redistribution of heat to the value of signal could be minimized, and the characteristic time of heating up of the membrane, and, accordingly, establishment of signal, could be estimated as the value $\sim c\rho a^2/\kappa \approx 7 \cdot 10^{-7}$ s. Cooling down of the bolometer after the end of the radiation pulse generally occurs due to the heat loss from the membrane via thin carrier bars having low thermal conductivity. The cooling down time or heat relaxation time of the bolometer $\tau = C/G$ for typical bolometers is ~ 10 ms [26], by exceeding many times the membrane heating up time τ_d, and, therefore, determining its fast action: the value of temperature response of the bolometer to the measured radiation pulse will be low dependent on the previous radiation pulse, if the time interval between them would be higher or about 3τ.

Figure 6, *b* shows electronic microscope image of the test microbolometer conjugated to a quasi-spiral antenna and made on the multiplexor with the pixel size $51 \times 51\,\mu$m. The antenna occupies the area of 3×3 pixels, and the microbolometer is connected to the multiplexor in the central pixel of each array 3×3 [18]. At the same time, one should note that in order to increase sensitivity and

quick response of the bolometer, it is more beneficial to use microbolometers of a smaller size, e.g. $25 \times 25\,\mu$m, that, versus microbolometers with the size of $51 \times 51\,\mu$m, have about 4 times lower thermal capacity. It is because the rate of response of the bolometer to short ($t_{pe} \ll \tau$) pulsed radiation $T(t_2) - T(t_1) \approx Q_S/C$ is inversely related to its thermal capacity, and the cooling down time of the bolometer $\tau = C/G$ is pro rata to its thermal capacity. In this design, the antenna is located on sacrificial layer, the thickness of which could amount to $\sim 2-5\,\mu$m. For the purpose of the antenna performance optimization, the same as in the studies [7–9], a thick layer of dielectric material (e.g., silicon oxide or nitride with the thickness of $\sim 10\,\mu$m or higher) could be applied between the sacrificial layer and the silicon pad. Having taken the resistance of the load and each busbar of the resistance link r equal to 100 and 15 Ω, accordingly, we will find, that the portion of the Joule heat released in the load when absorbing the radiation pulse is 70%. At the same time, according to the Wiedemann–Franz law, the thermal conductivity of the resistance link busbars caused by the charge carriers, $G_e = 2LT_C/r$, will make $1.0 \cdot 10^{-6}$ W/K. Here, L is the Wiedemann–Franz constant equal to $2.45 \cdot 10^{-8}\,\mathrm{W\Omega/K^2}$, and T_C is the temperature of the pad, which we take equal to 300 K. The full thermal conductivity of the bolometer G will be a bit higher due to, first, thermal conductivity of the metal lattice, which for the metals with high electrical conductivity (such as Au, Cu, Ag, Al) could be low versus the electron thermal conductivity [27,28], and, second, thermal conductivity via the bearing bars with metallic busbars connecting the thermally sensitive element of the bolometer to the signal reading scheme, the typical value of which is less than $1.0 \cdot 10^{-7}$ W/K [29–31], which are not taken into account here. As a result, subject to the value of the thermal capacity of the membrane C for microbolometers having the size $25-28\,\mu$m that could be $\sim 4 \cdot 10^{-10}$ J/K [29–31], let's find the thermal relaxation time of the bolometer $\tau = C/G \approx 0.4$ ms and, therefore, such a bolometer must be capable to measure the energy of each of the radiation pulses following one another at the frequency of $\sim 1/3\tau \approx 830$ Hz.

By measuring the bolometer signal (immediately after arrival of the radiation pulse) by applying the pulsed voltage bias of the bolometer $V_D \approx 2$ V within the time of integration of the signal $\tau_i \approx 30\,\mu$s, and having treated the signal value $V_{SI} = \alpha(0.7Q_S/C)V_D \approx \approx \alpha(0.7\eta Q_{SI}/C)V_D$ as a full noise of the measurement scheme (reduced to the bolometer), which, in general, is $\sim 10\,\mu$V [32,33], we can estimate the minimum resolved energy of radiation pulse falling onto the bolometer $Q_{SI} \approx 3 \cdot 10^{-13}$ J. Here, η is coefficient of absorption of the THz radiation taken as 0.5 (over 80% of the falling radiation is absorbed by the antenna [8,9] and 70% of that energy is released in the resistive load) and α is TCR of the bolometer, which, the same as earlier, is taken equal to -2%/K [2]. For comparison, we state that average powers of radiation of a photoconductive antenna and THz quantum-cascade laser are about 0.1 mW [13] and 10 mW [34]. The energies of one pulse with the duration of 100 μs will be 10^{-8} and 10^{-6} J, accordingly, thus enabling to get a snapshot THz image with the signal/noise ratio ≈ 40 on matrices with the format 32×24 and 320×240, accordingly.

In order to provide the snapshot mode, one may use the direct injection multiplexor, similar to those applicable in the studies [35,36], where in each cell of the photosensitive matrix the „dark" current is deducted, with further integration of the difference in the reserve capacity. Because, versus the studies [35,36], in our case we must perform the measurement for less time than $\tau \approx 0.4$ ms, e.g., for 30 μs, in order to ensure the root mean square Johnson noise is less than $10\,\mu$V, one must use the bolometers with the resistance below 300 kΩ. Subject to ensuring the deduction of not less than 95% „dark" current, to perform integration of the signal of bolometers with the resistance of 100–300 kΩ the reserve capacity $C_i \approx 3-10$ pF charged not less than up to 3 V is enough. Such a value of the capacity could be implemented in the multiplexor with the use of field silicon oxide with the thickness of 15 nm. The capacitor area will be not more than $37 \times 37 - 75 \times 75\,\mu$m, which is expedient for the terahertz radiation detectors, because in this case the pixel size determined by the antenna size could be $100 \times 100\,\mu$m and more. The compensating „dark" current could be specified by application of either reference bolometers (senseless to the measured radiation, e.g., made without antenna) [37], or current mirrors [38] placed in each cell of the MMBD. Note also that for the matrix detector with the format 160×120 at the frame rate of 1000 Hz the bit timing frequency of the output signal will be 20 MHz (or 5 MHz with 4 output channels available), which will not put challenges in terms of the circuitry engineering.

Conclusion

The study dealt with the dependence of the bolometer signal on the duration, shape and period of radiation pulses, as well as on the thermal relaxation time of the bolometer. We obtained analytical ratios for the temperature response of the bolometers to periodic radiation pulses of three different shapes: rectangular, triangular and the Gauss one. It was shown theoretically and based on the example with the infrared bolometers it was ascertained experimentally that the temperature response is determined by the thermal capacity of the bolometer and has a low dependence on its thermal conductivity, provided that the radiation pulse duration is far less than their period and the time of thermal relaxation of the bolometer. Such feature allows application, for registration of short IR and THz pulses, of the bolometer designs characterized in a high thermal conductivity and, therefore, a low time of thermal relaxation, thus making them fast acting without decreasing the sensitivity. In particular, it was shown, that microbolometers with the resistance-linked and thermally uninsulated antenna, having

a high thermal conductivity and a low sensitivity to the constant intensity radiation, can be high efficient for registration of the THz pulsed radiation. Based on such bolometers one could develop uncooled matrix detectors of the pulsed THz radiation, characterized in a minimum detectable energy of less than $1 \cdot 10^{-12}$ J and the frame rate up to 1000 Hz. The approach considered above may also be applied to the bolometer detectors of millimeter radiation.

Funding

The study has been performed under the state assignment №0242-2021-0007.

Conflict of interest

The authors declare that they have no conflict of interest.

Appendix

In general case, when efficient radiation pulse duration t_{pe} could be compared to the time of thermal relaxation τ, the values $DT(t_1, t)$ and $DT(t_1, t_2)$ forming part of the expressions (5)–(7), for three types of pulses specified by the ratios (8) and shown in Fig. 1, can be expressed analytically:

1) for rectangular pulse:

$$DT_1(t_1, t) = \frac{Q_S}{C} \frac{1}{(t_p/\tau)} [\exp(t/\tau) - \exp(-t_p/2\tau)], \quad \text{at} \quad t_1 < t < t_2, \tag{A1a}$$

$$DT_1(t_1, t_2) = \frac{Q_S}{C} \frac{\mathrm{sh}(t_p/2\tau)}{t_p/2\tau}, \tag{A1b}$$

where $t_1 = -t_p/2$, $t_2 = t_p/2$;

2) for triangular pulse:

$$DT_2(t_1, t) = \frac{Q_S}{C} \frac{1}{(t_p/2\tau)^2} \left[\exp\left(-\frac{t_p}{2\tau}\right) - \exp\left(\frac{t}{\tau}\right) + \left(\frac{t_p}{2\tau} + \frac{t}{\tau}\right) \exp\left(\frac{t}{\tau}\right)\right], \quad \text{at} \quad t_1 < t < 0, \tag{A2a}$$

$$DT_2(t_1, t) = \frac{Q_S}{C} \frac{1}{(t_p/2\tau)^2} \left[\exp\left(-\frac{t_p}{2\tau}\right) + \exp\left(\frac{t}{\tau}\right) - 2 + \left(\frac{t_p}{2\tau} - \frac{t}{\tau}\right) \exp\left(\frac{t}{\tau}\right)\right], \text{ at } 0 < t < t_2, \tag{A2b}$$

$$DT_2(t_1, t_2) = \frac{Q_S}{C} 2 \frac{\mathrm{ch}(t_p/2\tau) - 1}{(t_p/2\tau)^2}. \tag{A2c}$$

where $t_1 = -t_p/2$, $t_2 = t_p/2$;

3) for the Gauss pulse:

$$DT_3(t_1, t) = \frac{Q_S}{C} \frac{1}{2} \left\{1 + \mathrm{erf}\left[\frac{1}{\sqrt{2}} \left(\frac{t}{t_p/b} - \frac{t_p/b}{\tau}\right)\right]\right\} \times \exp\left[\frac{(t_p/b)^2}{2\tau^2}\right], \quad \text{at} \quad t_1 < t < t_2, \tag{A3a}$$

$$DT_3(t_1, t_2) = \frac{Q_S}{C} \exp\left[\frac{(t_p/b)^2}{2\tau^2}\right], \tag{A3b}$$

where $t_1 = -n(t_p/2)$, $t_2 = n(t_p/2)$, $n \geq 1$ and $\mathrm{erf}(x)$ are the function of errors.

Note that dependences shown in Fig. 2, calculated with the use of integral (7) and analytical (P1)–(P3) ratios at $n = 1.5$, coincide to the accuracy of the line width. At the same time, it should be highlighted that the ratios (P1) and (P2) are accurate, and (P3) is approximate. The accuracy of the latter increases as far as the parameter n is growing. At $n = 1$ and 1.5 relative power of radiation $P_S(t_1)/P_S(0) = P_S(t_2)/P_S(0)$ at the extremes of the interval (t_1, t_2) is $4.3 \cdot 10^{-2}$ and $8.5 \cdot 10^{-4}$, accordingly.

References

[1] A. Rogalski. Progress in Quantum Electronics, **36** (2–3), 342 (2012). DOI: 10.1016/j.pquantelec.2012.07.001
[2] F. Niklaus, C. Vieider, H. Jakobsen. Proc. SPIE, **6836**, 68360D (2007). DOI: 10.1117/12.755128
[3] A. Rogalski. Opto–Electron. Rev., **21** (4), 406 (2013). DOI: 10.2478/s11772-013-0110-x
[4] A.W.M. Lee, B.S. Williams, S. Kumar, Q. Hu, J.L. Reno. IEEE Photonics Technol. Lett., **18** (13), 1415 (2006). DOI: 10.1109/LPT.2006.877220
[5] N. Oda. C.R. Physique, **11** (7–8), 496 (2010). DOI: 10.1016/j.crhy.2010.05.001
[6] M.A. Dem'yanenko, D.G. Esaev, B.A. Knyazev, G.N. Kulipanov, N.A. Vinokurov. Appl. Phys. Lett., **92** (13), 131116 (2008). DOI: 10.1063/1.2898138
[7] N. Nemoto, N. Kanda, R. Imai, K. Konishi, M. Miyoshi, S. Kurashina, T. Sasaki, N. Oda, M. Kuwata-Gonokami. IEEE Trans. on Terahertz Sci. Technol., **6** (2), 175 (2016). DOI: 10.1109/TTHZ.2015.2508010
[8] F. Simoens, J. Meilhan. Philosophical Transactions of the Royal Society of London A: Mathematical, Physical and Engineering Sciences, **372** (2012), 20130111 (2014). DOI: 10.1098/rsta.2013.0111
[9] F. Simoens, J. Meilhan, J.-A. Nicolas. J. Infrared Milli Terahz Waves, **36**, 961 (2015). DOI: 10.1007/s10762-015-0197-x
[10] G.S. Kent, B.R. Clemesha, R.W. Wright. J. Atmospheric Terrestrial Phys., **29** (2), 169 (1967). DOI: 10.1016/0021-9169(67)90131-6
[11] G.S. Kent, R.W. Wright. J. Atmospheric Terrestrial Phys., **32** (5), 917 (1970). DOI: 10.1016/0021-9169(70)90036-X
[12] C.W. Berry, M.R. Hashemi, M. Jarrahi. Appl. Phys. Lett., **104** (8), 081122 (2014). DOI: 10.1063/1.4866807
[13] D.S. Kim, D.S. Citrin. Appl. Phys. Lett., **88** (16), 161117 (2006). DOI: 10.1063/1.2196480
[14] H. Hirori, A. Doi, F. Blanchard, K. Tanaka. Appl. Phys. Lett., **98** (8), 091106 (2011). DOI: 10.1063/1.3560062
[15] M.A. Belkin, F. Capasso. Phys. Scr., **90** (11), 118002 (2015). DOI: 10.1088/0031- 8949/90/11/118002
[16] L. Li, L. Chen, J. Zhu, J. Freeman, P. Dean, A. Valavanis, A.G. Davies, E.H. Linfield. Electron. Lett., **50** (4), 309 (2014). DOI: 10.1049/el.2013.4035
[17] Q. Lu, M. Razeghi. Photonics, **3** (3), 42 (2016). DOI: 10.3390/photonics3030042
[18] M.A. Dem'yanenko, D.G. Esaev, V.N. Ovsyuk, B.I. Fomin, A.L. Aseev, B.A. Knyazev, G.N. Kulipanov, N.A. Vinokurov. J. Opt. Technol., **76** (12), 739 (2009). DOI: 10.1364/JOT.76.000739

[19] D. Dufour, L. Marchese, M. Terroux, H. Oulachgar, F. Généreux, M. Doucet, L. Mercier, B. Tremblay, C. Alain, P. Beaupré, N. Blanchard, M. Bolduc, C. Chevalier, D.D'Amato, Y. Desroches, F. Duchesne, L. Gagnon, S. Ilias, H. Jerominek, F. Lagacé, J. Lambert, F. Lamontagne, L.L. Noc, A. Martel, O. Pancrati, J.-E. Paultre, T. Pope, F. Provençal, P. Topart, C. Vachon, S. Verreault, A. Bergeron. J. Infrared Milli Terahz Waves, **36** (10), 922 (2015). DOI: 10.1007/s10762-015-0181-5
[20] S. Zwerdling, R.A. Smith, J.P. Theriault. Infrared Phys., **8** (4), 271 (1968). DOI: 10.1016/0020-0891(68)90036-5
[21] *Handbook of Optics. Vol. I. Fundamentals, Techniques and Design, ed. by M. Bass, E.W. Van Stryland, D.R. Williams, W.L. Wolfe. — 2nd ed.* (McGraw-Hill, NY.–San Francisco–Washington, D.C. — etc, 1995).
[22] A.D. Polyanin, V.F. Zaitsev. *Handbook of Exact Solutions for Ordinary Differential Equations* (Chapman & Hall/CRC, Boca Raton–London–NY.–Washington, D.C. 2003)
[23] M.A. Dem'yanenko, A.F. Kravchenko, V.N. Ovsyuk. Avtometriya, **41** (5), 108 (2005) (in Russian).
[24] V.Sh. Aliev, M.A. Dem'yanenko, D.G. Esaev, I.V. Marchishin, V.N. Ovsyuk, B.I. Fomin. Uspekhi prikladnoi fiziki, **1** (4), 471 (2013) (in Russian).
[25] M.A. Dem'yanenko, B.I. Fomin, L.L. Vasilieva, S.A. Volkov, I.V. Marchishin, D.G. Esaev, V.N. Ovsyuk, V.L. Dshkhunyan, E.B. Volodin, A.V. Ermolov, P.P. Usov, V.P. Chesnokov, Yu.S. Chetverov, P.N. Kudryavtsev, A.E. Zdobnikov, A.A. Ignatov. Prikladnaya fizika, **4**, 124 (2010) (in Russian).
[26] P. Eriksson, J.Y. Andersson, G. Stemme. J. Microelectromechanical Systems, **6** (1), 55 (1997).
[27] C. Kittel. *Introduction to Solid State Physics, 8th Edition.* (John Wiley and Sons, NY., 2005)
[28] F.H. Schofield. Proceed. Royal Society A: Mathematical, Phys. Engineer. Sci., **107** (742), 206 (1925). DOI: 10.1098/rspa.1925.0016
[29] F. Niklaus, A. Decharat, C. Jansson, G. Stemme. Infrared Phys. Technol., **51** (3), 168 (2008). DOI: 10.1016/j.infrared.2007.08.001
[30] M. Kohin, N. Butler. Proc. SPIE, **5406**, 447 (2004). DOI: 10.1117/12.542482
[31] J.J. Yon, A. Astier, S. Bisotto, G. Chamingís, A. Durand, J.L. Martin, E. Mottin, J.L. Ouvrier-Buffet, J.L. Tissot. Proc. SPIE, **5783**, 432 (2005). DOI: 10.1117/12.606487
[32] D. Svard, C. Jansson, A, Alvandpour. Analog Integr Circ Sig Process, **77** (1), 29 (2013). DOI: 10.1007/s10470-013-0116-9
[33] A. Tanaka, K. Chiba, T. Endoh, K. Okuyama, A. Kawahara, K. Iida, N. Tsukamoto. Proc. SPIE, **4130**, 160 (2000). DOI: 10.1117/12.409858
[34] B.S. Williams. Nature Photon., **1** (9), 517 (2007). DOI: 10.1038/nphoton.2007.166
[35] C.H. Hwang, C.B. Kim, Y.S. Lee, H.C. Lee. Electron. Lett., **44** (12), 732 (2008). DOI: 10.1049/el:20080879
[36] S. Ajmera, J. Brady, C. Hanson, T. Schimert, A.J. Syllaios, M. Taylor. Proc. SPIE, **8012**, 80121L (2011). DOI: 10.1117/12.884249
[37] J.L. Tissot, C. Trouilleau, B. Fieque, A. Crastes, O. Legras. Opto-Electron. Rev., **14** (1), 25 (2006). DOI: 10.2478/s11772-006-0004-2
[38] F. Simoens, M. Tchagaspanian, A. Arnaud, P. Imperinetti, G. Chammings, J.J. Yon, J.L. Tissot. Proc. SPIE, **6542**, 65421T (2007). DOI: 10.1117/12.719310